RR Lyrae Stars and Stellar Evolution in the Globular Cluster M15

Ryan Rubenzahl[1,*] and Bo Peng[1,†]

[1] *Department of Physics and Astronomy, University of Rochester, Rochester, New York, USA*

(Dated: October 12, 2017)

We present lightcurves for 30 RR Lyrae variable stars identified in the globular cluster M15 using observations recorded at the University of Rochester's C.E.K. Mees Observatory. The periods of the variables are compared to observations of the brightest RR Lyrae star, RR Lyrae itself, whose proximity is such that its distance is accurately determined by parallax measurements. From this we estimate the distance to M15 to be 9000 ± 370 pc. Further, we perform photometry for the stars in the cluster in three wavelength bands and present a HR diagram of M15. We discuss the evolution of the stellar members of M15 by comparison of the HR diagram to that of nearby stars.

PACS numbers: 98.20.Gm, 95.85.Kr, 97.30.Kn, 97.10.Vm, 97.10.Zr
Keywords: Mees Observatory, Messier 15, M15, globular cluster, RR Lyrae, variable star, HR Diagram

I. INTRODUCTION

RR Lyrae stars are a class of variable star commonly found in globular clusters. RR Lyraes are old, population II stars that have burned through all of their hydrogen and passed through the red-giant branch phase of stellar evolution. As such, these stars are found in the horizontal branch of the Hertzsprung-Russell (HR) diagram. Like the Cepheid variables, their variability in brightness is due to pulsations caused by the κ-mechanism and is closely related to its absolute magnitude, making these types of stars well-suited for use as standard candles in measuring distances within our galaxy.

An exact period-luminosity relation for RR Lyrae stars is not well-defined at visible wavelengths, but is in the IJHK infrared range of the Johnson-Cousins-Glass system. A theoretical relation in the visible range exists based on the metallicity of the star [1]. The period is dependent on the star's mass, luminosity, and temperature, which do not follow precise relations. In the context of our analysis, we assume the composition of stars with similar periods to the prototypical RR Lyrae star, RR Lyrae itself, to be the same, implying a similar absolute magnitude. As RR Lyrae is close enough to the Solar System to have its distance accurately measured by parallax [2], a rough estimate of the distance to the globular cluster M15 can be made.

The Hertzsprung-Russell (HR) diagram is a scatter plot between two intrinsic properties of stars: magnitude (related to luminosity), and color, the difference between magnitudes in two wavelength bands (related to temperature). The typical HR diagram is made by plotting the Johnson V band magnitude (increasing downwards) against the color index B - V of the Johnson B (λ_0 430, $\Delta\lambda$ 100 nm) and V (λ_0 540, $\Delta\lambda$ 90 nm) bands. To emulate this style of HR diagram with the Mees CCD filterset, we will plot the G magnitude vs. B - R (see Table I for wavelength bands). Regions of the HR diagram are populated in 'clusters' that correspond to different stages of stellar evolution. Most stars fall along a long strip from top-left to bottom-right known as the main sequence. Older stars that were once on the main sequence but burned through all their hydrogen move into the giant phase and along the red giant branch, and some giant stars (e.g. RR Lyrae's and Cepheids) migrate to the instability strip where they pulsate, causing their brightness to fluctuate over time.

Plotting a HR diagram for stars in a globular cluster reveals the history of the cluster, and tells the stories of the lives of the stars within it. Globular clusters tend to be very old ($\gtrsim 10$ billion years), and so most of the stars in the cluster will have evolved beyond the main sequence and into the giant phase. As such the brightest members of a globular cluster will populate the red giant branch and asymptotic giant branch, with the remaining main sequence members being fainter and less-easily detected.

II. C.E.K. MEES OBSERVATORY

The C.E.K. Mees Observatory is an astronomical observatory owned and operated by the University of Rochester 40 miles south of Rochester in Naples, New York ($77^\circ\,24'\,56''$ W, $42^\circ\,42'\,01''$ N, 701 m (2260 ft) altitude). The observatory, dedicated May 8, 1965, hosts open tours to the public over the summer months, and serves as the primary teaching instrument in observational astronomy to physics and astronomy students throughout the academic year. The observatory hosts a Boller and Chivens Cassegrain reflector with a 61 cm (24 in, 2700 cm^2 collecting area) primary mirror and 8229 mm (324 in) focal length.

Currently installed on the telescope is a Santa Barbara Instrument Group (SBIG) STX-16803 CCD camera (36.8 mm $\times$ 36.8 mm, 4096 $\times$ 4096 pixels at 9 μm, 15.4 arcmin square field-of-view) with 16-bit output that reads

* rrubenza@u.rochester.edu
† bpeng6@u.rochester.edu

Filter	λ_0 [nm]	$\Delta\lambda$ [nm]
R	637	125
G	535	90
B	445	110

TABLE I: Baader L-RGB CCD filterset wavelengths.

1.27 electrons per data number (DN)[1]. The main CCD has a 9 electron read noise and 0.009 electron/sec dark current at -20 °C, and is complemented by a STX Guider CCD (657 × 495 pixels at 7.4 μm) that is used for autoguiding on faint guide stars accompanying the observed target. In front of the CCD is a filter wheel containing five 50 mm square Baader color filters: Luminance (L), Red (R), Green (G), Blue (B), and Hα. Table I gives center-wavelength and bandwidth values for the L-RGB filters.

Commands are issued to the telescope from the control room located on the first level of the observatory using the DFM Engineering Telescope Control System (TCS) and planetarium software *TheSky6*. The CCD is controlled using the software *CCDSoft*.

III. OBSERVATIONS

The Mees Observatory site enjoys fairly dark sky conditions that average $\sim$ 2 arcsecond seeing on clear nights. Our observing runs cover three consecutive nights from 09/10/17 - 09/12/17 (Julian Day (JD) 2458006 - 2458008), and 09/22/17 (JD 2458018).

An observing run involves arriving at the observatory approximately one hour before sunset to allow sufficient time to start-up and synchronize the telescope and TCS software before taking flat-field data. Flat-field data consists of imaging the uniform-light twilight sky with the telescope pointed at zenith in short-enough exposures so as to not saturate the CCD (saturation is DN $\geq$ 65536 per pixel) but still provide a sufficient signal (30,000-40,000 DN). We take 32 exposures in each L-RGB filter, which are then individually combined to produce a 'master' flat-field frame for each wavelength filter. See Section IV for a more detailed discussion on the flat-field calibration process.

A. Targets

Once flat-field images are acquired and the sky has become sufficiently dark, we begin imaging our science targets. These are the globular cluster M15 (NGC 7078), the variable star RR Lyrae (SAO 48421), and several A0 V stars for flux calibration. Our main calibration star is SAO 126221 (HD 198070, A0 V, $m = 6.38$), which we observe each night except 09/10/17. We also include observations of SAO 126222 (09/11, A0 V, $m = 5.58$), SAO 107474 (09/10, 09/22, A0 V, $m = 5.69$), and SAO 88944 (09/10, A0 V, $m = 4.80$). The calibration stars are chosen based on their proximity to main targets (M15 and RR Lyrae) using the A0 star catalog compiled by the University of Hawaii Institute for Astronomy[2]. Table V in Appendix B shows the sequence of imaging for each night.

IV. DATA REDUCTION AND CALIBRATION

A. Dark/Bias/Flat-Field Calibration

The first step of reducing our data involves calibration of flat-field frames, dark current, and bias. Flat-field images account for the pixel-to-pixel variation in capacitance of the CCD, and allows for the correction of vignetting as well as removing dust specks on the color filters and the CCD array itself. Dark current refers to pixels recording a current in the absence of any input, and bias refers to the residual charge left behind at the end of an exposure due to imperfections of the switches that output the accumulated charge. These effects are measured by taking a large number of dark frames (zero-light input, 64 frames at 30 min each) and bias frames (256 frames of a given exposure time) for a given CCD temperature and binning, which are then averaged to produce "master dark/bias" frames [3]. Professor Dan M. Watson produced these master frames at the beginning of the summer, so they are still good to use for our data.

We use the software *CCDStack* to carry out the process of flat-fielding and dark/bias subtracting our images to produce output images that are corrected for these systematic effects. During this process we also reject hot/cold pixels and interpolate those removed from the image, so as to not mistake defective pixels as physical sources. *CCDStack* nicely automates this process for us given the input master dark/bias frames (for CCD temperature and binning) and master flat-field (for color filter and binning). The flat-fielded, dark/bias subtracted set of images for each target are then aligned by selecting alignment stars in *CCDStack*'s `Register` feature. The images are first manually (very roughly) aligned, and are then roughly aligned by *CCDStack*. A very fine alignment is achieved in *CCDStack* using a Bicubic B-spline routine.

We also normalize the images of M15 individually for R, G, and B to the first series of images taken on 09/22/17, using *CCDStack*'s `Normalize` feature. We do this so that we may flux-calibrate all the M15 images using the 09/22 calibration data, which is the most reliable calibration data we obtained.

[1] 1 DN is the unit of the CCD readout "count."

[2] http://irtfweb.ifa.hawaii.edu/IRrefdata/Catalogs/bsc_a0.dat

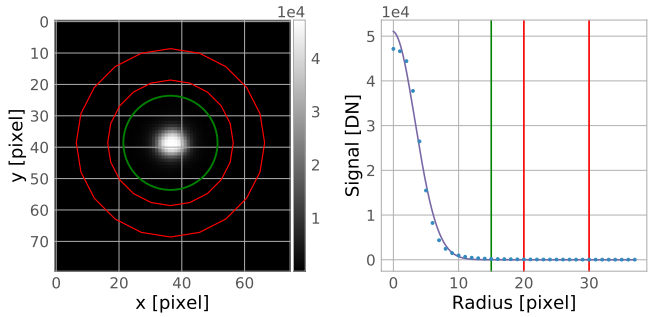

FIG. 1: Aperture photometry on the calibration star SAO 126221 on 09/12/17 for an image in the G filter. (Left): The `CircularAperture` (green) and `CircularAnnulus` (red) objects are defined around the star. (Right): Radial profile of the star signal with a Gaussian fit to estimate the point-spread-function. The radii of the apertures are denoted by the vertical lines.

B. Flux Calibration

The next step of calibration involves the conversion of the signal in DN to a signal in real flux units. To do this, we need to account for atmospheric attenuation of the measured signal. The amount of atmospheric attenuation depends on the amount of atmosphere the signal is passing through. For observations well above the horizon, the observed flux decreases with increasing zenith angle (ZA) according to [3]

$$f = f_0 - f_0 \tau_0 \sec(\mathrm{ZA}), \tag{1}$$

where f_0 is the flux at the 'top' of the atmosphere and τ_0 is the vertical optical depth. $\sec(\mathrm{ZA})$ is usually referred to as the "airmass."

To correct for this, we measure the signal from our calibration star at varying zenith angles to identify the best fit of Eq. 1 to our data. We do this for each night individually to account for variations in the weather. For each calibration star image, we perform aperture photometry to determine the total signal in DN from the star. This is done using the `astropy`-affiliated package `photutils` [4]. A `photutils.aperture.CircularAperture` object defines a circular region surrounding the star, within which the signal from each pixel is summed. The background is estimated using a `photutils.aperture.CircularAnnulus` object to identify an annulus surrounding the star, within which the signal is assumed to be background-only. The aperture sum within the annulus is normalized to the area of the circular aperture to estimate the background inside the circular aperture, and is then subtracted from the circular aperture sum to give the total star signal (in DN). Fig 1 gives an example of what this looks like.

The aperture radii are chosen by considering the radial profile of the star's signal and locating where the star's signal is most nearly completely enclosed (Fig 1).

Date	Filter	$\hat{f}_0$ [DN]	$\sigma_{\hat{f}_0}$ [DN]	$\hat{\tau}_0$	$\sigma_{\hat{\tau}_0}$
09-11-17	R	1.26×10^7	9.01×10^5	0.639	0.005
09-12-17	R	3.81×10^6	9.07×10^5	0.141	0.140
09-22-17	R	5.04×10^6	6.06×10^5	0.134	0.065
09-11-17	G	1.40×10^7	3.97×10^5	0.655	0.001
09-12-17	G	1.24×10^7	1.07×10^6	0.557	0.016
09-22-17	G	5.82×10^6	5.49×10^5	0.204	0.045
09-11-17	B	2.53×10^6	1.47×10^6	0.532	0.094
09-12-17	B	1.07×10^7	9.32×10^5	0.547	0.017
09-22-17	B	4.73×10^6	3.84×10^5	0.147	0.043

TABLE II: Best-fit parameters with uncertainties for atmospheric attenuation.

A Gaussian profile is fit to this to estimate the FWHM (full-width-half-maximum) of the signal. The FWHM estimate for all observations of the calibration star are averaged together to be used later as a seed to locate stars in our images of M15.

We estimate the uncertainty in the signal using `photutils.utils.calc_total_error`, which considers the Poisson statistical uncertainty in the counts[3] as well as the 1σ fluctuation of the background σ_b. This gives an error per-pixel in the number of DN observed by

$$\sigma = \sqrt{\sigma_b^2 + 1.27 \cdot \mathrm{DN}}. \tag{2}$$

The error in the total signal is then found using error propagation from each of the pixels that went into the sum.

It turns out that this error is extremely small compared to the population variance in the observed signal for each series, as seen in Fig 2. The signal of the calibration star is on the order of 10^6, and so the errors found in Eq. 2 are on the order of $\sqrt{10^6} = 10^3$. Thus these uncertainties may be considered negligible, and in future calculations we only consider the population variance in quantifying of error. We use the Levenberg-Marquardt least squares algorithm from `scipy.optimize.curve_fit` to fit Eq. 1. The results of the fit are tabulated in Table II.

C. Converting DN to Flux

A0 V stars have the useful property that their color index is zero for any two visible-range wavelengths, and are thus the same magnitude across the visible range. This allows proper scaling of one standard star which has a magnitude of zero in the visible range (Vega) to all other A0 V stars of different magnitudes. The Johnson photometric bands for Vega, a zero-magnitude A0 V star, have the corresponding flux values shown in Table III.

[3] Counts = number of electrons read, i.e. 1.27·DN, since that is what is being 'counted' by the CCD.

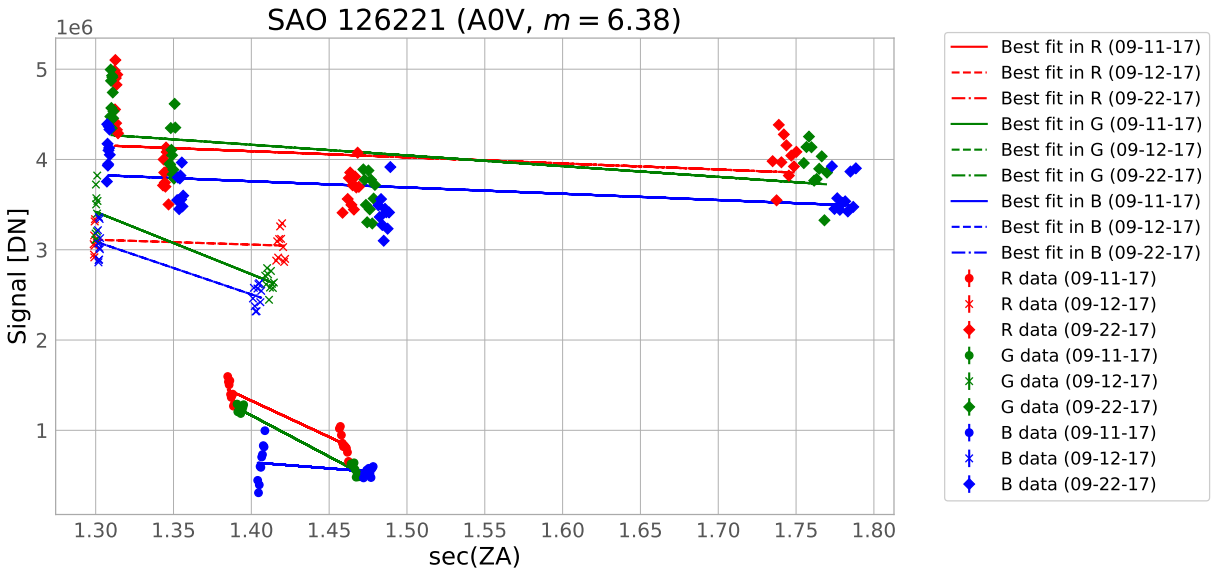

FIG. 2: Observed signal in DN as a function of airmass for SAO 126221. Each night is fit individually to account for differences in weather. The images taken on 09/10 appear shifted lower due to a shorter exposure time used.

Filter	λ_0 [μm]	$\Delta\lambda$ [μm]	ν_0 [Hz]	F_λ [W cm^{-2} μm^{-1}]	F_ν [W m^{-2} Hz^{-1}]	log F_ν [F_ν in W m^{-2} Hz^{-1}]
U	0.36	0.07	8.3×10^{14}	4.35×10^{-12}	1.88×10^{-23}	-22.73
B	0.43	0.10	7.0×10^{14}	7.20×10^{-12}	4.44×10^{-23}	-22.36
V	0.54	0.09	5.6×10^{14}	3.92×10^{-12}	3.81×10^{-23}	-22.42
R	0.70	0.22	4.3×10^{14}	1.76×10^{-12}	2.88×10^{-23}	-22.54

TABLE III: Spectral flux density in the Johnson UBVR photometric bands for Vega [3, 5].

Since Vega has $m = 0$, the flux measured from the calibration star is

$$f_c = f_{\text{Vega}} 10^{-m_c/2.5} = F_\lambda \Delta\lambda_{\text{Mees}} 10^{-m_c/2.5}, \quad (3)$$

for a given color filter. To convert DN to flux, consider the "DN flux," DN/(AT) where T is the exposure time and A is the collection area of the Mees primary mirror. We then scale DN to the true flux f_0 by

$$f \propto \frac{\text{DN}}{AT} \;\Rightarrow\; f = f_c \frac{\text{DN(ZA)}}{\text{DN}_c\text{(ZA)}} \frac{T_c}{T}, \quad (4)$$

since the collection area A is the same. The signal from the calibration star DN_c is determined by

$$\text{DN}_c(\text{ZA}) = \hat{f}_0 - \hat{f}_0 \hat{\tau}_0 \sec(\text{ZA}) \quad (5)$$

where $\hat{f}_0$ and $\hat{\tau}_0$ are the best-fit parameters for the given color filter/date in Table II, and ZA is the zenith angle of the source being converted. The true signal of the source, DN_0, is given by the attenuation-correction of the measured signal, DN, by

$$\text{DN}_0 = DN/\left(1 - \hat{\tau}_0 \sec(\text{ZA})\right) \quad (6)$$

Eq. 4 can then be used to convert an image in DN to an equivalent image in real flux units (erg / s / cm^2), where all the fluxes are corrected to their value at the top of the atmosphere.

V. RR LYRAE VARIABLES

A. RR Lyrae

To understand the properties of the RR Lyrae stars in M15, we first have to consider RR Lyrae itself (SAO 48421). We recorded observations of RR Lyrae periodically throughout the nights, between exposures of M15, in an attempt to observe the brightness of RR Lyrae change as it pulsates (see Appendix B for our full imaging sequence). To do this, we create a lightcurve (plot brightness vs. time) of RR Lyrae to look for periodicity in the brightness.

We use the same procedure for measuring the flux from RR Lyrae as in Section IV B with the calibration star, with the alteration of using `photutils.psf.BasicPSFPhotometry` (see Section VII for a detailed discussion of PSF photometry in Python). We do this for each series of images and record the mean magnitude observed for each series. In this case, a weighted mean is used to account for the error in the

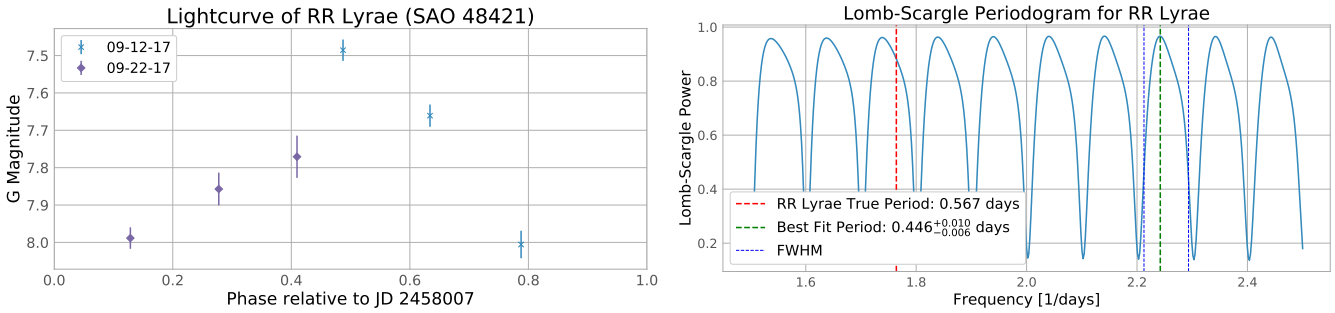

FIG. 3: (Left): Lightcurve of RR Lyrae (G magnitude vs. time in Julian Day) phased by the known period. (Right): Periodogram of RR Lyrae with the known period marked by the dashed red line. No clear periodicity is detected.

observed signal, which itself is calculated via error propagation from all the pixels going into the sum, which each have error given by Eq. 2. Series with poor seeing are removed from the analysis: 09/22 series 4, and 09/10 and 09/11 are removed entirely due to the unreliable flux-calibration from those nights (not enough observations of calibration stars). The lightcurve we produce is shown in Fig 3.

RR Lyrae varies in magnitude from $m = 7.06$ to $m = 8.12$ in a 0.56686776 day period [6]. Due to our limited sample size of data (6 points after cuts, spread over two nights a week apart) we only seek to confirm variability on this scale. To do so we employ a Lomb-Scargle periodogram test to our lightcurve (`astropy.stats.LombScargle`). Lomb-Scargle periodograms work well with data that is non-uniformly sampled in time, however we have too few data points that also contain a time-gap much larger than the average time between data points, and thus the periodogram fails to detect significant periodicity at any one frequency. Instead, we phase the data to the known period relative to our first night of data (09/10, JD 2458007) to observe the general shape of the lightcurve with high and low-points of brightness, between 7th and 8th magnitude as expected. We can also estimate the maximum apparent magnitude (corresponding to minimum flux) of RR Lyrae from this data, yielding $\max(m_G) = 8.17 \pm 0.129$.

The distance to RR Lyrae has been accurately determined from parallax measurements taken by the *Gaia* spacecraft [2]. *Gaia* measures a parallax of 3.6386 ± 0.2335 mas for RR Lyrae, which corresponds to a distance of 274.828 ± 0.064 pc.

From this distance we can determine the absolute magnitude of RR Lyrae via

$$M_G = m_G - 5 \log \left(\frac{d}{10 \text{ pc}} \right). \tag{7}$$

We find $\max(M_G) = 0.976 \pm 0.128$. In our analysis of the RR Lyrae population of M15, we will assume that those with similar periods to RR Lyrae share the same absolute magnitude.

B. RR Lyrae Variables in M15

We identify variable stars in our images of M15 "the old-fashioned way," by blinking color images and looking for variables by eye[4]. *CCDStack* contains a feature to blink between images at the user's desired rate, and also allows one to determine the centroid coordinates of a given star by double-clicking on it (with the images static, so that both the clicks are registered in one image), which initiates a quick point-spread-function (PSF) fit to the the clicked location. We compile a list of 31 unique variable candidates in this manner.

The positions of each of these candidates are cross-referenced with the results of photometry on the entire M15 cluster (Section VII). 30 candidates are confirmed to match to an identified star, and one lone candidate is not matched, due to being located outside the cropped region of the M15 images that we consider in Section VII. The coordinates of the matched candidates (in both pixel x/y and RA (α)/Dec (δ) are displayed in Table IV.

For each variable candidate, the same PSF photometry analysis used for RR Lyrae is conducted. To identify a small region around the star and to fit the star's flux, we use an initial guess of 10 pixels for the full-width-half-maximum (FWHM). The analysis of the variable candidates consists of applying a loop over the variable candidates, and for each candidate:

1. Identify a 6x6 (in units of FWHM) region around the star.
2. Then, for each image of M15:
   - i Estimate the background in the cropped region.
   - ii Use `photutils.psf.BasicPSFPhotometry` to fit the star, taking the location of the variable to be fixed.
   - iii Correct the resulting flux (in DN) for atmospheric attenuation.

[4] A blinking gif of our 09/22 images can be found at `http://www.pas.rochester.edu/~rrubenza/09-22-17-color-series.gif`

ID	x [pixel]	y [pixel]	α (J2000)	δ (J2000)	$\bar{m}_G$	max(m_G)	Period [day]	p-value
V 01	1528.2600	1224.5800	21h29m17.124s	+12°02'59.671"	14.996 ± 0.031	15.293 ± 0.128	$0.752^{+0.017}_{-0.015}$	0.0122
V 02	1302.7900	1146.3700	21h29m23.840s	+12°03'32.644"	14.700 ± 0.038	15.125 ± 0.161	$0.950^{+0.028}_{-0.037}$	0.0009
V 03	1146.8100	944.5500	21h29m28.557s	+12°05'01.029"	15.201 ± 0.033	15.699 ± 0.138	$0.693^{+0.016}_{-0.010}$	0.0035
V 04	1404.4300	684.1100	21h29m21.072s	+12°06'58.641"	15.230 ± 0.030	15.650 ± 0.127	$0.696^{+0.014}_{-0.010}$	0.0003
V 05	1694.8800	1857.5900	21h29m11.865s	+11°58'19.945"	15.213 ± 0.030	15.769 ± 0.127	$1.136^{+0.023}_{-0.051}$	0.0018
V 06	940.0500	1803.2000	21h29m34.233s	+11°58'38.241"	15.229 ± 0.030	15.805 ± 0.127	$1.277^{+0.030}_{-0.065}$	0.0000
V 07	753.4100	1271.6200	21h29m40.034s	+12°02'32.782"	15.203 ± 0.031	15.790 ± 0.129	$0.519^{+0.007}_{-0.007}$	0.0000
V 08	628.7500	1303.7500	21h29m43.704s	+12°02'17.556"	15.184 ± 0.031	15.752 ± 0.128	$0.537^{+0.007}_{-0.008}$	0.0000
V 09	459.7700	1241.5900	21h29m48.735s	+12°02'43.840"	14.941 ± 0.031	15.544 ± 0.127	$0.686^{+0.016}_{-0.017}$	0.0375
V 10	971.0900	1001.0300	21h29m33.728s	+12°04'34.593"	15.109 ± 0.031	15.681 ± 0.130	$1.280^{+0.035}_{-0.078}$	0.0003
V 11	1013.3400	889.8400	21h29m32.534s	+12°05'24.286"	14.959 ± 0.031	15.365 ± 0.130	$0.866^{+0.016}_{-0.027}$	0.0000
V 12	897.1500	864.9500	21h29m35.991s	+12°05'34.427"	15.247 ± 0.031	15.602 ± 0.128	$0.387^{+0.004}_{-0.004}$	0.0074
V 13	778.0700	740.3700	21h29m39.580s	+12°06'28.813"	15.158 ± 0.031	15.534 ± 0.128	$1.051^{+0.044}_{-0.042}$	0.0000
V 14	784.1500	748.4000	21h29m39.397s	+12°06'25.297"	15.226 ± 0.031	15.732 ± 0.128	$1.196^{+0.066}_{-0.038}$	0.0000
V 15	1052.4900	1421.9600	21h29m31.106s	+12°01'28.361"	15.273 ± 0.036	15.812 ± 0.157	$0.738^{+0.017}_{-0.016}$	0.0215
V 16	1062.7300	1359.4600	21h29m30.835s	+12°01'56.184"	14.963 ± 0.065	15.526 ± 0.466	$1.351^{+0.045}_{-0.030}$	0.0029
V 17	957.2800	979.6600	21h29m34.153s	+12°04'43.973"	15.174 ± 0.032	15.729 ± 0.133	$0.811^{+0.017}_{-0.017}$	0.0000
V 18	1120.4300	1064.6400	21h29m29.275s	+12°04'07.512"	15.123 ± 0.041	15.733 ± 0.190	$0.577^{+0.008}_{-0.008}$	0.0000
V 19	1380.5800	1249.0700	21h29m21.482s	+12°02'47.651"	15.134 ± 0.033	15.729 ± 0.140	$1.277^{+0.032}_{-0.075}$	0.0000
V 20	1334.9800	1256.7500	21h29m22.830s	+12°02'43.892"	15.220 ± 0.041	15.829 ± 0.189	$0.763^{+0.012}_{-0.012}$	0.0000
V 21	1210.4500	1600.0900	21h29m26.338s	+12°00'10.509"	15.199 ± 0.031	15.801 ± 0.129	$0.701^{+0.015}_{-0.011}$	0.0008
V 22	1357.4900	1713.8400	21h29m21.929s	+11°59'21.146"	15.177 ± 0.031	15.767 ± 0.129	$0.981^{+0.040}_{-0.017}$	0.0000
V 23	1290.6500	1485.5400	21h29m24.023s	+12°01'01.980"	15.220 ± 0.032	15.637 ± 0.132	$1.049^{+0.042}_{-0.045}$	0.0005
V 24	1200.5500	1414.9800	21h29m26.726s	+12°01'32.604"	15.011 ± 0.040	15.684 ± 0.184	$0.595^{+0.010}_{-0.011}$	0.0000
V 25	1117.4700	1792.3300	21h29m28.989s	+11°58'44.445"	15.029 ± 0.030	15.455 ± 0.128	$1.066^{+0.051}_{-0.030}$	0.0000
V 26	990.1400	1298.4800	21h29m33.010s	+12°02'22.695"	14.879 ± 0.038	15.466 ± 0.169	$0.691^{+0.016}_{-0.013}$	0.0000
V 27	858.4100	1221.8300	21h29m36.951s	+12°02'55.702"	15.151 ± 0.032	15.745 ± 0.135	$0.600^{+0.009}_{-0.009}$	0.0000
V 28	853.1800	1380.3200	21h29m37.024s	+12°01'45.301"	15.259 ± 0.031	15.496 ± 0.130	$0.223^{+0.001}_{-0.001}$	0.0275
V 29	997.3100	1352.4800	21h29m32.776s	+12°01'58.776"	15.129 ± 0.045	15.568 ± 0.196	$0.748^{+0.015}_{-0.016}$	0.0126
V 30	969.7600	1351.3500	21h29m33.589s	+12°01'59.068"	14.948 ± 0.035	15.461 ± 0.150	$0.806^{+0.016}_{-0.020}$	0.0135

TABLE IV: Variable stars identified in M15.

iv Convert the corrected flux (in DN) to true flux (in W / cm^2).

v Convert flux to apparent magnitude.

vi Estimate the uncertainty in the magnitude from the fluctuation of the background, propagating through steps iii - v, accounting for all other uncertainties.

vii Save the apparent magnitude and its error to a list, along with the Julian Date (JD) of the observation.

Then, for each variable, the time series of apparent magnitudes is used to compute the Lomb-Scargle periodogram in order to identify the best-fit period. We estimate the uncertainty in the best-fit period by taking the frequencies above and below the best-fit frequency corresponding to half of the maximum power. To estimate the significance of the peak in Lomb-Scargle power (LSP), we calculate a p-value for the hypothesis of no time variation given the observed peak. We do this by repeating the following procedure for 5000 iterations to adequately sample the parameter space:

1. Shuffle the time data, effectively washing out any supposed periodic signal.

2. Calculate a Lomb-Scargle periodogram for the shuffled data.

3. Identify the peak in the periodogram, and save the value of the peak LSP to a list.

We histogram the resulting LSP peaks to estimate the distribution of observed peaks, and calculate from the histogram the p-value (integrated tail-probability). The p-value is estimated by a trapezoidal sum of the histogram bins corresponding to LSP values $\geq$ the observed peak. See Fig 5 for an example periodogram and resulting histogram for one of the variable candidates analyzed. The resulting p-values for each variable candidate,

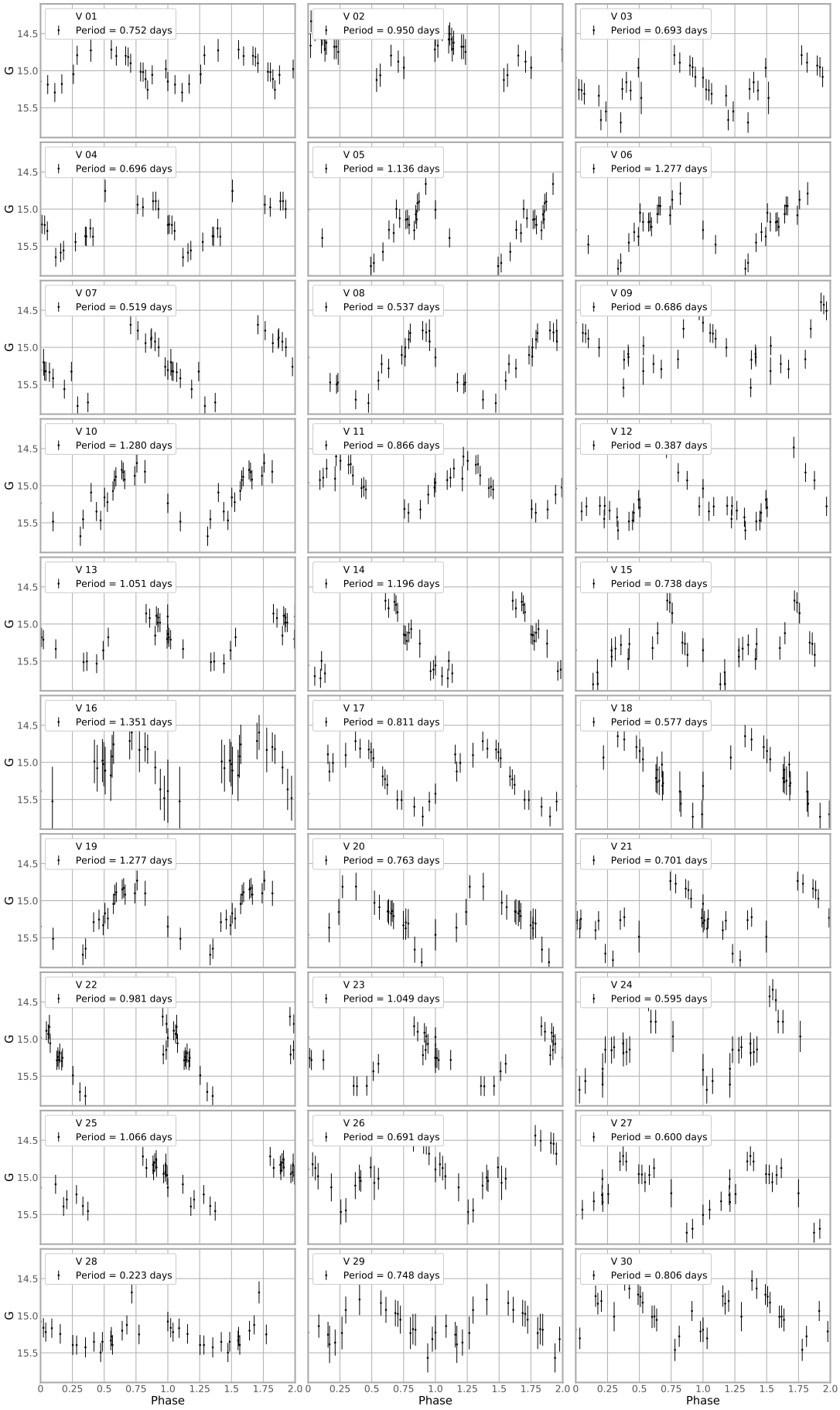

FIG. 4: Lightcurves for the 30 variable stars identified within M15.

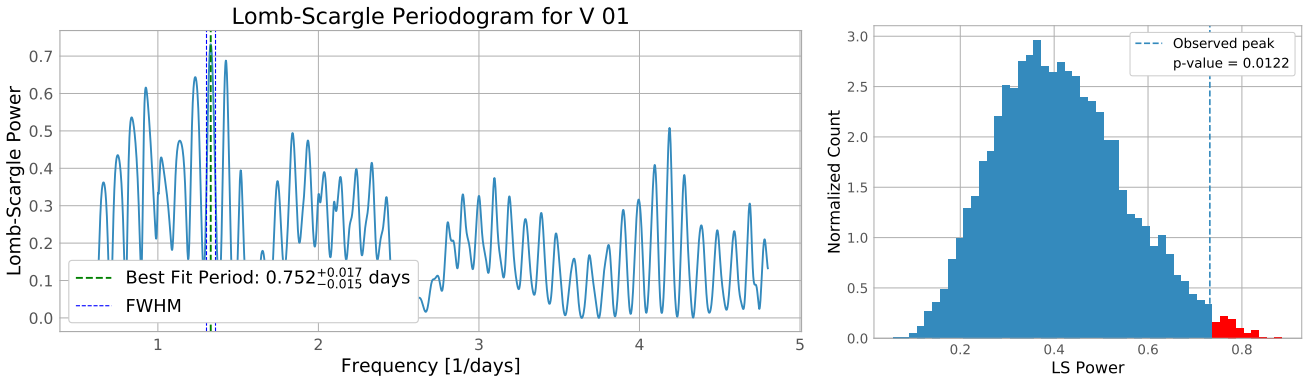

FIG. 5: (Left): Periodogram for variable candidate V 01. (Right): Histogram of peak LSP for 5000 randomly shuffled versions of the data. The observed peak is denoted by the dashed vertical line.

along with the best-fit period, are given in Table IV as well. All variable candidates analyzed have periodicity detected with p-value < 0.05.

From the best-fit period, we calculate the period-folded times to plot the lightcurve as a function of the phase of the variable's period. To aid visual inspection, and in good practice with the convention for plotting RR Lyrae lightcurves, the data are duplicated over two phases to better display the variability. The collection of lightcurves for all 30 variable candidates are displayed in Fig 4.

All 30 variables are identified (positionally) with previous observations of M15 as known RR Lyrae stars [6, 7]. Due to our small sample-size and limited time resolution, most of our periods do not match the reported periods but are instead a multiple of two or three times the previously reported period. This is likely due to the Lomb-Scargle algorithm seeking the Nyquist frequency, which for our sparse data may appear as a signal with a longer period than actually is true. More observations to fill in the time-gaps would improve our time-resolution and increase our sensitivity to these shorter periods.

C. Distance to M15

Assuming the RR Lyrae stars we have identified in the M15 globular cluster are identical to RR Lyrae in absolute magnitude, we can compute the distance to M15 by rearranging Eq. 7 for d,

$$d = 10^{(\mathrm{DM}+5)/5}, \tag{8}$$

where $\mathrm{DM} = m_G - M_G$ is the distance modulus. Letting M_G be the maximum apparent magnitude for RR Lyrae as calculated in Section V A, and letting m_G be the maximum magnitude measured for each variable star, we compute the distance to each of the variable stars in M15 that exhibit a similar period to RR Lyrae: we take only the periods that are within 10% of RR Lyrae's. Since all the variables are contained in the cluster, we may combine these distances to estimate the distance to M15:

$$d = 9000 \pm 370 \text{ pc}. \tag{9}$$

The accepted distance to M15 is around 10 kpc, which is $\sim 2.5\sigma$ from our estimate. Our estimate is likely to have been biased low due to an underestimate of the maximum magnitude observed for each variable, for which we have limited data.

VI. PHOTOMETRY OF THE M15 CLUSTER

To be able to plot the HR diagram for M15, we need to perform PSF photometry on the entire cluster. This involves identifying stars in the image and determining their flux. A number of powerful functions exist in `astropy` and `photutils` to do this, although they are (as warned in the documentation) currently experimental. To avoid issues with blank data around the edges of the image (a side-effect from the alignment process), and to avoid source confusion from the bright star HD 204712 to the north of M15, we crop the data to a 1500×1500 square region centered on M15.

We begin by estimating the background of our M15 image. This is done using a `photutils.background.Background2D` object which uses sigma-clipped statistics to estimate the background (considering pixels only below a given sigma threshold) in square regions of 10×10 pixels throughout the entire image, and then blending these regions together to create a background map that is allowed to vary in both dimensions. To improve the accuracy of the background estimation, a source mask is passed to the `Background2D` object to remove potential sources from consideration in the background estimation. The source mask eliminates any grouping of 50 pixels or more that each have a signal-to-noise ratio (SNR) of 5 or greater. Fig 6 shows the result of the background subtraction.

The next step involves locating stars in the image. We use the DAOPHOT algorithm developed

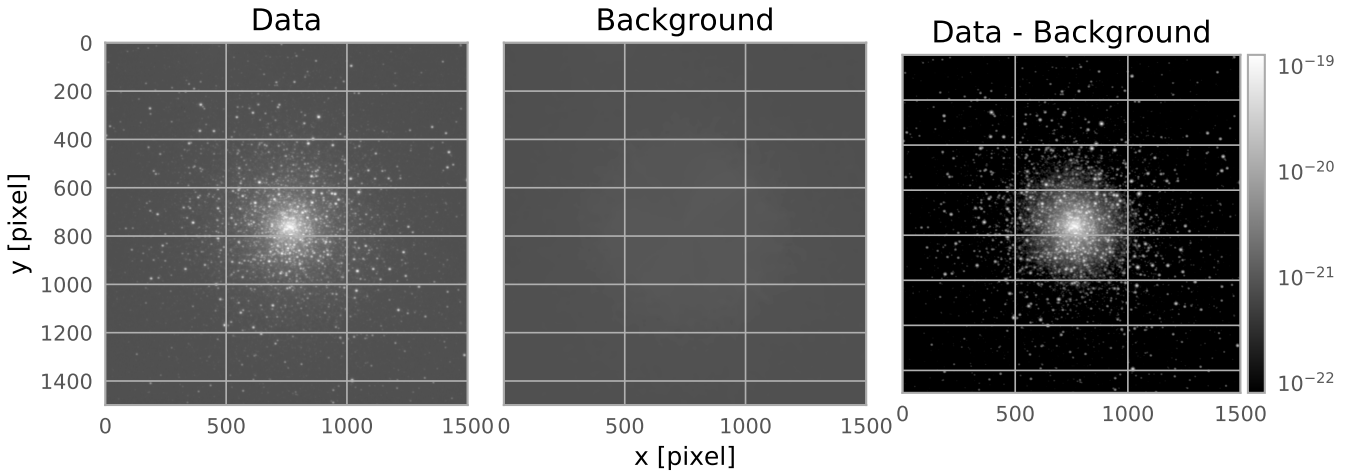

FIG. 6: Background-subtraction of the M15 data. The color-scale corresponds to flux in units of W cm^{-2}.

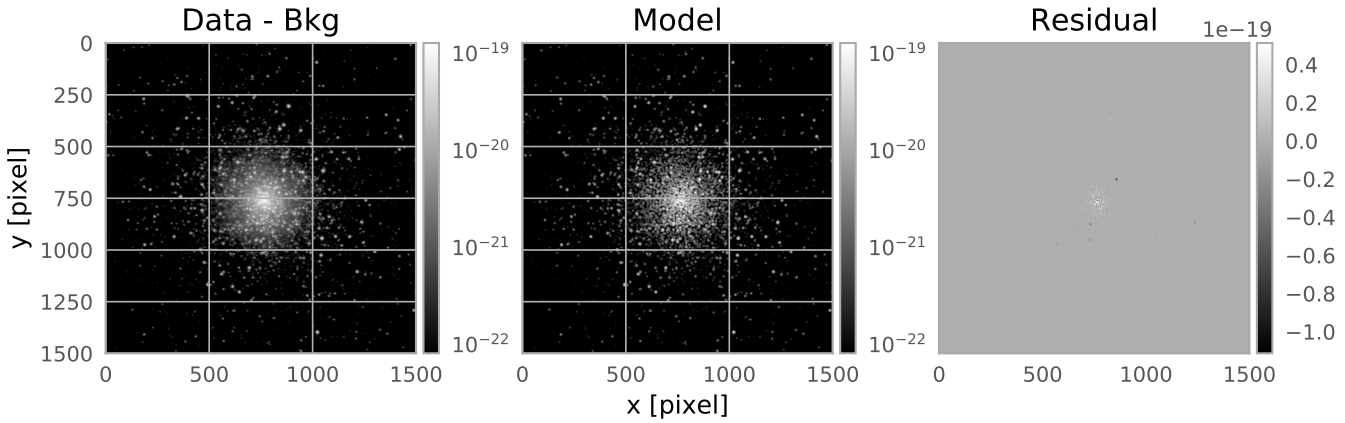

FIG. 7: Example model image for M15. The model is composed of a Gaussian source at the location of each identified star and with the amplitude and width given by the best-fit PSF model. The residual plot is generated by subtracting the model from the Data - Bkg image. A few stars near the center can be seen to have been over-subtracted, and a small amount of the unresolved core is leftover. Color-scale units are W cm^{-2}.

by [8], which is implemented in `photutils.psf` as `IterativelySubtractedPSFPhotometry`. The algorithm consists of applying the following loop over the image:

1. Locate stars using IRAFStarFinder, which identifies local density maxima above a specified threshold.
2. Group sources to be fit simultaneously (using `photutils.psf.DAOGroup`).
    - This effectively reduces the dimensionality of the task of fitting thousands of stars each modeled by several parameters to instead fit the groups of stars simultaneously.
3. Fit groups: x and y centroid location and flux.
4. Subtract the fitted groups from the image.

This loop is repeated for a specified number of iterations or until no more stars are found. We use just one iteration, as further iterations tend to produce lots of negative stars (the first iteration over-subtracts the actual star, leaving a negative peak in the residual for the second iteration to pick up), and the grouping algorithm has trouble fitting stars even if these negative anomalies are removed (the large quantity of 'stars' it claims to find in the second iteration cause overlap issues with the groups).

We use the IRAFStarFinder routine just once, on the stacked R image, to generate a list of stars. This list of stars is used to generate a model of M15, with all the anomalies removed (negative x or y centroid or negative flux). The model is generated by injecting a Gaussian source at the location of each star according to the best-fit PSF found by `IterativelySubtractedPSFPhotometry`. Fig 7 shows

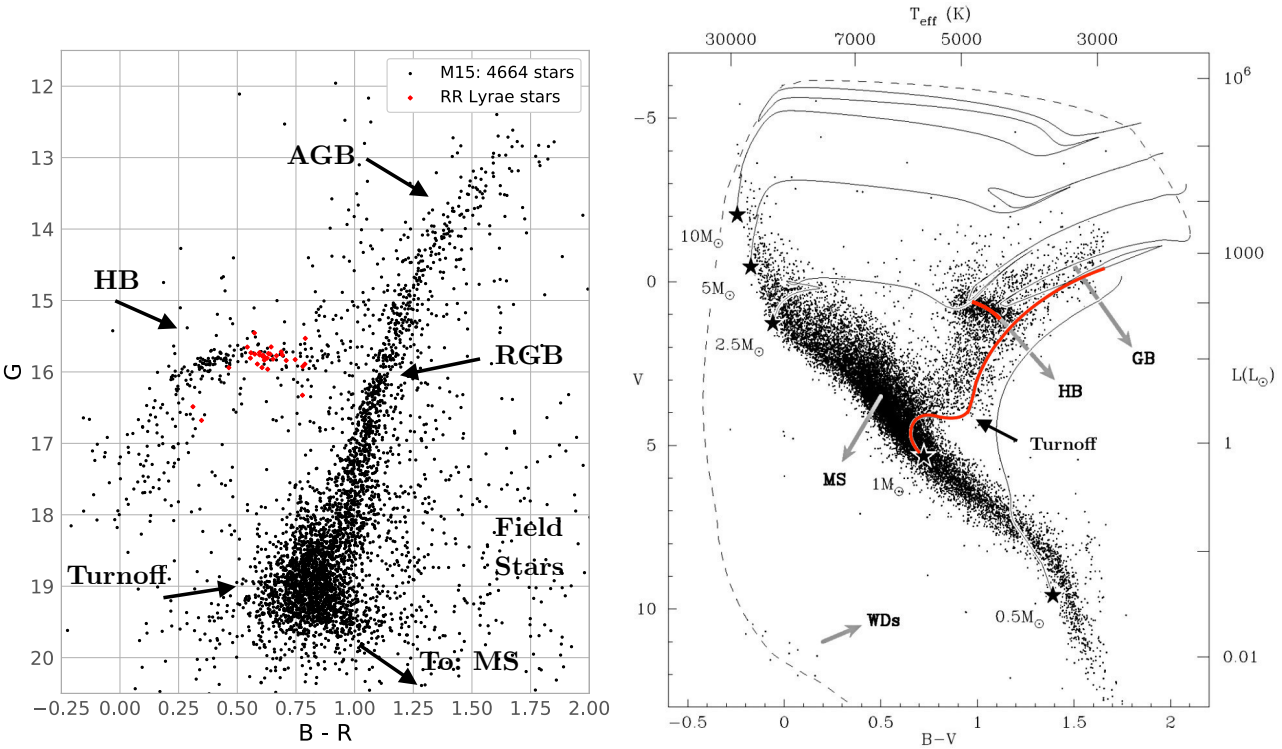

FIG. 8: (Left): Our color-magnitude (HR) diagram of M15, annotated. (Right): HR diagram of nearby stars with stellar evolution tracks traced for several masses of main sequence stars. Credit: Wikipedia Commons.

an example of the model generated for the R image with the resulting residual image.

The star positions from the model are then used to define a PSF model for the stars with fixed positions. We use `photutils.psf.IntegratedGaussianPRF` for our PSF model, which treats the flux from each star as a circular 2D Gaussian integrated over the pixels. We then use this model to fit just the flux of the stars for each of the three stacked R, G, and B images of M15. From these fluxes, we calculate the stellar magnitudes in each wavelength band and plot G vs. the color index B - R. This yields the HR diagram shown in Fig 8. The color-magnitude location of the RR Lyrae stars we identified in Section V are highlighted by the red points in the HR diagram.

VII. HR DIAGRAM OF M15

We plot G vs. B-R to create a diagram of closest appearance to the Johnson V vs. B-V plot. The asymptotic giant branch (AGB) is seen in the upper-right, the main 'trail' of stars being the Red Giant Branch (RGB), and the horizontal branch (HB) is clearly identified to the left (where the RR Lyrae stars live). The diagram cuts off just after the main-sequence turnoff (MS-TO) point, which would extend the trail of stars towards dimmer (∼24th magnitude) and redder stars: the main-sequence.

As can be seen by the highlighted evolution track for a 1 $M_\odot$ main sequence star in the full HR diagram in Fig 8, the end of the main-sequence star's hydrogen burning phase sees it brighten and move upwards, around the turnoff (indicated by the arrow) and becomes brighter and redder. This is the red giant phase, where the star begins to burn helium, swelling in size. As the star consumes its supply of helium, it either moves further along this track towards the end of the giant branch where it undergoes helium flash, a stage where the rest of the star's helium is quickly consumed and the star gets very bright and very hot before fading away into a white dwarf (dashed-line track in the diagram), or the composition of the star becomes such that light emitted from the interior is blocked by the outer atmosphere of the star, causing the star to swell. As the star swells, the outer atmosphere becomes diffuse and the light is allowed to escape, and the star contracts. This is the κ-mechanism, and stars that pulsate from this move off the giant branch and into the horizontal branch along the instability strip: this is where the variable stars like the RR Lyrae stars we detected live.

Looking at the shape of our HR diagram and the relative B-R values[5], we can see that our diagram corre-

[5] Note that our y-axis is apparent magnitude, whereas the y-axis of the V vs. B-V plot is absolute magnitude. This is to pro-

sponds to highlighted region of the full HR-diagram containing the red giant branch, asymptotic giant branch, and horizontal branch. This indicates that the stars in M15 have aged well-beyond the main sequence and are now almost entirely in the giant stages of stellar evolution. Since $1M_\odot$ main sequence stars have lifetimes on the order of 10 Gyr, the age of the M15 must be at least that old. Thus stars are not eternal; they go through stages of evolution as they age until, eventually, they exhaust all their fuel and are left cold and dark for the rest of time.

VIII. SUMMARY

From observations recorded at the University of Rochester's C.E.K. Mees Observatory between 09/10/17 and 09/22/17, 30 RR Lyrae variable stars are identified in the globular cluster M15. Lightcurves for each of the variables are presented after phasing to the best-fit period obtained from a Lomb-Scargle periodogram test. Measurements of the periods of each of the variables are combined with measurements of the prototype RR Lyrae star, RR Lyrae, to estimate the distance to the globular cluster M15. We found the distance to be 9000 ± 370 pc. From photometry of the stars in the cluster, a HR diagram of M15 is produced, and stellar evolution is observed among the cluster's members. This paper is submitted in partial fulfillment of the requirements of PHY 243W: Advanced Experimental Techniques at the University of Rochester.

ACKNOWLEDGMENTS

We especially wish to thank Professor Watson for his patience in teaching us everything we needed to know about the telescope and CCD imaging system, and for walking us through troubleshooting when the RA drive was oscillating in the middle of a long exposure!

This work has made use of data from the European Space Agency (ESA) mission *Gaia* (`https://www.cosmos.esa.int/gaia`), processed by the *Gaia* Data Processing and Analysis Consortium (DPAC, `https://www.cosmos.esa.int/web/gaia/dpac/consortium`). Funding for the DPAC has been provided by national institutions, in particular the institutions participating in the *Gaia* Multilateral Agreement.

[1] M. Catelan, B. J. Pritzl, and H. A. Smith, The Astrophysical Journal Supplement Series **154**, 633 (2004).

[2] Gaia Collaboration, A. G. A. Brown, A. Vallenari, T. Prusti, J. H. J. de Bruijne, F. Mignard, R. Drimmel, C. Babusiaux, C. A. L. Bailer-Jones, U. Bastian, and et al., Astronomy and Astrophysics **595**, A2 (2016), arXiv:1609.04172 [astro-ph.IM].

[3] D. Watson, "You, too, can make useful and beautiful astronomical images at Mees," CCD Lessons (2016).

[4] L. Bradley, B. Sipocz, T. Robitaille, E. Tollerud, Z. Vincius, C. Deil, K. Barbary, H. M. Gnther, M. Cara, M. Droettboom, A. Bostroem, E. Bray, L. A. Bratholm, T. E. Pickering, M. Craig, G. Barentsen, S. Pascual, adonath, J. Greco, W. Kerzendorf, StuartLittlefair, L. Ferreira, F. D'Eugenio, and B. A. Weaver, "astropy/photutils: v0.3," (2016).

[5] H. L. Johnson, Annual Review of Astronomy and Astrophysics **4**, 193 (1966).

[6] N. N. Samus', E. V. Kazarovets, O. V. Durlevich, N. N. Kireeva, and E. N. Pastukhova, Astronomy Reports **61**, 80 (2017).

[7] T. M. Corwin, J. Borissova, P. B. Stetson, M. Catelan, H. A. Smith, R. Kurtev, and A. W. Stephens, The Astronomical Journal **135**, 1459 (2008), arXiv:0802.2089.

[8] P. B. Stetson, Publications of the Astronomical Society of the Pacific **99**, 191 (1987).

vide easier cross-comparison of our M15 results with other observations/experiments, without inflicting the uncertainty in our distance measurement.

Appendix A: Color Image of M15

FIG. 9: RGB true color composite of M15 made from data taken on 09/22/17. This color image was produced in *CCDStack* by layering stacked exposures of R, G, and B with ratios 1 : 1.16 : 1.58 (to make an A0 V star appear white) and with background desaturated. Total exposure time = 40 min R, 40 min G, 64 min B.

Appendix B: Imaging Sequence

(a) 09/10 (2" seeing)

Target	Series	Filter	Exposure [s]	Time [UTC]
SAO107474	1	R	5 (×10)	09-11T02:00
		G	5 (×10)	
		B	5 (×10)	
SAO88944	1	R	2 (×10)	09-11T02:15
		G	2 (×10)	
		B	2 (×10)	
RR Lyrae	1	R	7 (×20)	09-11T02:30
		G	7 (×20)	
		B	7 (×20)	
M 15	1	R	300 (×1)	09-11T03:30
		G	300 (×1)	
RR Lyrae	2	R	10 (×20)	09-11T05:45
		G	10 (×20)	
		B	10 (×20)	
	3	R	10 (×10)	09-11T05:45
		G	10 (×10)	
		B	10 (×10)	
M 15	2	R	300 (×1)	09-11T07:00
		G	300 (×1)	
		B	300 (×4)	

(b) 09/11 (2" seeing)

Target	Series	Filter	Exposure [s]	Time [UTC]
SAO126221	1	R	5 (×10)	09-12T01:00
		G	5 (×10)	
		B	5 (×10)	
SAO126222	1	R	5 (×10)	09-12T01:15
		G	5 (×10)	
		B	5 (×10)	
RR Lyrae	1	R	7 (×10)	09-12T01:30
		G	7 (×10)	
		B	7 (×10)	
M15	1	R	300 (×3)	09-12T02:15
		G	300 (×3)	
		B	300 (×6)	
RR Lyrae	2	R	7 (×10)	09-12T04:15
		G	7 (×10)	
		B	7 (×10)	
SAO126221	2	R	5 (×10)	09-12T04:30
		G	5 (×10)	
		B	5 (×10)	
RR Lyrae	3	G	10 (×10)	09-12T05:30
	4	G	15 (×10)	09-12T06:00

(c) 09/12 (1.5" seeing)

Target	Series	Filter	Exposure [s]	Time [UTC]
SAO126221	1	R	5 (×10)	09-13T00:45
		G	5 (×10)	
		B	5 (×10)	
RR Lyrae	1	G	7 (×20)	09-13T01:00
M15	1	R	300 (×3)	09-13T02:00
		G	300 (×3)	
		B	300 (×6)	
SAO126221	2	R	5 (×10)	09-13T03:00
		G	5 (×10)	
		B	5 (×10)	
RR Lyrae	2	G	7 (×20)	09-13T03:00
M15	2	R	300 (×3)	09-13T04:00
		G	300 (×3)	
		B	300 (×6)	
SAO126221	3	R	5 (×10)	09-13T05:00
		G	5 (×10)	
		B	5 (×10)	
RR Lyrae	3	G	7 (×20)	09-13T05:15
M15	3	R	300 (×3)	09-13T06:00
		G	300 (×3)	
		B	300 (×6)	
SAO126221	1	R	5 (×10)	09-13T07:15
		G	5 (×10)	
		B	5 (×10)	

(d) 09/22 (1.5" seeing)

Target	Series	Filter	Exposure [s]	Time [UTC]
RR Lyrae	1	G	7 (×20)	09-23T01:00
SAO126221	1	R	7 (×10)	09-23T01:15
		G	7 (×10)	
		B	7 (×10)	
M15	1	R	480 (×2)	09-23T02:00
		G	480 (×2)	
		B	480 (×4)	
SAO126221	2	R	7 (×10)	09-23T03:00
		G	7 (×10)	
		B	7 (×10)	
RR Lyrae	2	G	7 (×10)	09-23T03:15
SAO126221	3	R	7 (×10)	09-23T03:45
		G	7 (×10)	
		B	7 (×10)	
RR Lyrae	3	G	7 (×10)	09-23T04:45
M15	2	R	480 (×1)	09-23T04:15
		G	480 (×1)	
		B	480 (×2)	
SAO126221	4	R	7 (×10)	09-23T04:45
		G	7 (×10)	
		B	7 (×10)	
M15	3	R	480 (×1)	09-23T05:30
		G	480 (×1)	
		B	480 (×2)	
SAO107474	1	R	7 (×10)	09-23T06:00
		G	7 (×10)	
		B	7 (×10)	
RR Lyrae	4	G	7 (×10)	09-23T06:15
M15	4	R	480 (×1)	09-23T06:30
		G	480 (×1)	

TABLE V: Sequence of imaging for each night.